The effect of vocal fold vertical stiffness variation on voice production

Biao Geng, Qian Xue, and Xudong ZhengZZ

Citation: The Journal of the Acoustical Society of America **140**, 2856 (2016); doi: 10.1121/1.4964508
View online: http://dx.doi.org/10.1121/1.4964508
View Table of Contents: http://asa.scitation.org/toc/jas/140/4
Published by the Acoustical Society of America

The effect of vocal fold vertical stiffness variation on voice production

Biao Geng, Qian Xue,[a] and Xudong Zheng
Department of Mechanical Engineering, University of Maine, Orono, Maine 04473, USA

(Received 4 April 2016; revised 20 September 2016; accepted 26 September 2016; published online 21 October 2016)

A parametric study was conducted using the numerical technique that coupled a three-dimensional continuum vocal fold model with a one-dimensional Bernoulli flow model to investigate the effect of vocal fold vertical stiffness variation on voice production. Vertical stiffness gradient was defined as the ratio of the inferior–superior stiffness difference to the mean stiffness and was introduced in the cover layer. The results showed that increasing the vertical stiffness gradient would increase the peak flow rate and sound intensity and decrease the open quotient and threshold pressure. The effect was found to be more prominent at low subglottal pressures. The underlying mechanism might be that the reduced stiffness at the superior aspect of the vocal fold would allow a larger lateral displacement and result in a larger vibration. Increasing the vertical stiffness gradient was also found to increase the vertical phase difference and glottal divergent angle during the vocal fold vibration. Meanwhile, increasing the vertical stiffness variation only slightly increased the mean flow rate, which is important to maintaining the speech time between breaths.
 [http://dx.doi.org/10.1121/1.4964508]

[ZZ] Pages: 2856–2866

I. INTRODUCTION

Stiffness variation in the vertical direction on the vocal fold medial surface was recently reported. Using indentation, Chhetri *et al*. (2011) measured the Young's modulus on the medial surface of *ex vivo* human vocal fold samples. It was observed that the inferior medial surface was stiffer than the superior medial surface in both female and male samples across a wide range of ages. The average Young's modulus was 7.5 kPa at the inferior medial surface and 4.8 kPa at the superior medial surface. This variation was identified in both intact vocal folds separated from the laryngeal framework and combined epithelium and lamina propria layers dissected and separated from the vocal fold muscle. Chhetri *et al*. (2011) proposed that such variation of the stiffness was in accordance with the variation of the morphologic structure of vocal fold, i.e., the variation from the subglottic cricothyroid membrane to the lamina propria half way along the medial surface. The subglottic cricothyroid membrane, which is also called conus elasticus, is composed of dense fibro connective tissue with abundant elastic fibers. It extends from the upper border of the cricoid cartilage to the lower margin of the vocal ligaments, and attaches anteriorly to the thyroid cartilage and posteriorly to the vocal processes of the arytenoid cartilages (Reidenbach, 1996). Because of the gradual change of the morphologic structure, Chhetri *et al*. (2011) also suggested a gradual decrease in the stiffness from the inferior medial surface to superior medial surface. More recently, the same technique was repeated on more samples including 15 canine samples and two human samples (Chhetri and Rafizadeh, 2014). The softer-superior–stiffer-inferior variation in the stiffness was observed in all the samples. With the same technique, Oren *et al*. (2014a) systematically measured the Young's modulus of the canine vocal folds in intact larynges at both superior and inferior aspects. Their measurements also confirmed the softer-superior–stiffer-inferior variation in the stiffness. Furthermore, the measurements suggested that the stiffness variation increased with the normal strain from the indentation. They hypothesized that the larger stiffness variation under large strain was the cause of larger divergent angles observed in phonation under high subglottal pressures (Oren *et al*., 2014b). Therefore, it was proposed that it is important to maintain the stiffness gradient when performing clinical procedures such as laryngeal medialization as the stiffness gradient would increase the divergent angle during vibrations (Dembinski *et al*., 2013). However, this hypothesis has not been verified. It was also reported in the three-mass computational model that the vertical phase difference was promoted if the upper spring was slightly softer than the lower spring (Story and Titze, 1995); however, the mechanism was not well understood.

Nevertheless, while more measurements are needed to identify the causes of the vertical stiffness variation and to better quantify such feature, it is important to study the effect of the vertical stiffness variation on vocal fold dynamics and voice production. Such study would help to determine if the vertical stiffness variation is a beneficial feature for voice production; if so, how and to what extent it would affect voice production. The findings would be useful as a reference in tissue engineering and laryngeal surgeries such as medialization. The findings would also have implications for vocal fold modelling as the vertical stiffness variation might be an important feature to be included in phonation models.

[a]Electronic mail: qian.xue@maine.edu

II. METHODS

In this study, a continuum vocal fold model was coupled with a one-dimensional (1-D) Bernoulli flow to model the flow-structure interaction between the vocal fold and glottal flow. The modeling method is described below.

A. Vocal fold model

The geometry of the vocal fold (shown in Fig. 1) was adopted from Zheng *et al.* (2010). The two-dimensional (2-D) vocal fold profile was extracted from a high-resolution laryngeal CT scan of a normal male subject and was extruded in the anterior–posterior direction to generate the three-dimensional (3-D) model. The vocal fold was 1.5 cm long, 0.99 cm wide, 1.0 cm high, and the medial surface was about 0.3 cm high. The anterior surface, posterior surface and the lateral surface were fixed. The model assumed the left–right symmetry for simplicity and only the left vocal fold was simulated with the plane of symmetry set at $x = 0.99$ cm, making a zero initial glottal opening. The two-layer (body-cover) assumption was utilized to model the inner anatomical structure of the vocal fold. The cover layer started from the plane of $x = 0.85$ cm to the medial surface with a maximum thickness of 1.4 mm, which was approximately the combined thickness of the vocal fold epithelium and lamina propria (Chhetri *et al.*, 2011). Vocal fold tissues were modeled as viscoelastic transversely isotropic incompressible materials. The adopted material properties are listed in Table I. To provide a quantitative description of the stiffness variation, a vertical stiffness gradient (VSG) was defined as the ratio of the inferior–superior stiffness difference to the mean stiffness (E_0):

$$\mathrm{VSG}\,(\%) = \frac{E_{\mathrm{inf}} - E_{\mathrm{sup}}}{E_0} \times 100. \tag{1}$$

While introducing the VSG, it should be noted that the mean stiffness would also affect the vocal fold dynamics. So the same mean stiffness was desired to rule out its effect. To achieve this, the integral of the modulus along the y direction was kept same. The local modulus was calculated using the following equation:

TABLE I. Material properties of vocal fold tissues (Alipour *et al.*, 2000).

Property	Unit	Cover	Body
Transverse Young's modulus	kPa	2.014	3.99
Longitudinal Young's modulus	kPa	20	40
Longitudinal shear modulus	kPa	10	30
Transverse Poisson's ratio		0.9	0.9
Density	g/cm^3	1.2	1.2
Damping	poise	3	5

$$E(y) = E_0 - E_0 \frac{\mathrm{VSG}}{100} \frac{(y_c - y_{\mathrm{mid}})}{(y_1 - y_2)}, \tag{2}$$

where $E(y)$ is the local modulus, y_c is the y coordinate of the geometrical center of the element, y_1 and y_2 are the upper and lower vertical bound measured at the lateral–medial middle of the cover layer, respectively; y_{mid} is the vertical midpoint of the cover layer, which equals the average of y_1 and y_2. The vertical stiffness variation was introduced in the cover by implementing Eq. (2) to each individual element in the cover layer. We interpreted the measurements from the indentation method as a general measurement of stiffness, thus in each case all three moduli (transverse Young's modulus, longitudinal Young's modulus and longitudinal shear modulus) were varied simultaneously with the same gradient. The dynamics of the vocal fold was governed by the Navier equation and we solved the equation using the in-house finite element analysis (FEA) code with a linear elasticity formulation. Since left–right symmetry was assumed in this study, vocal fold contact was considered to occur when the vocal fold crossed the glottal midline. In this case, an additional contact pressure that was proportional to the degree of the penetration was applied along the lateral–medial direction to the surface nodes that crossed the midline. The contact pressure was calculated with the following equation:

$$p_c = \gamma K (x - x_{\mathrm{midline}}) \text{ if } x > x_{\mathrm{midline}}, \tag{3}$$

where p_c is the contact pressure, γ is the contact coefficient, K is the maximum coefficient in the global stiffness matrix in FEA formulas. The value of γ was set to be 9.34 for this study through trial and error. For the baseline case with 1.0 kPa subglottal pressure, the maximum penetration was

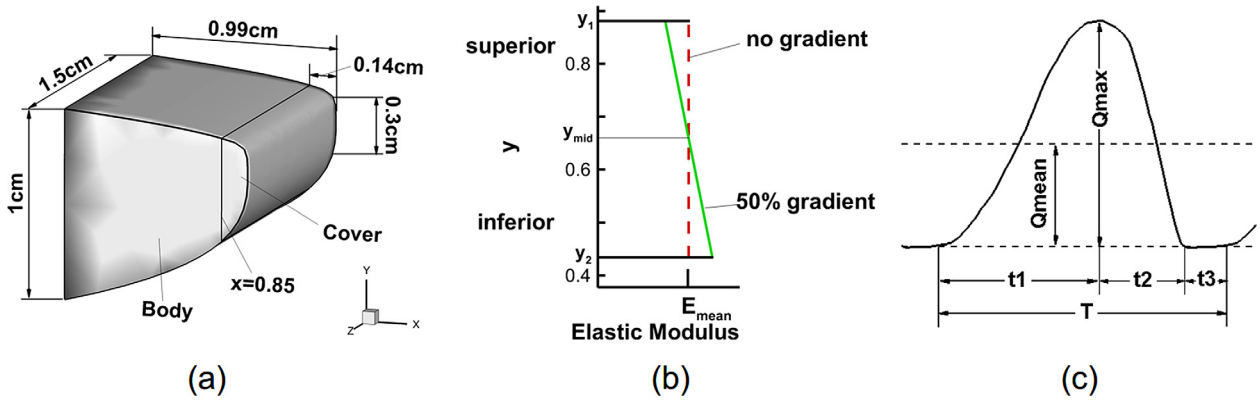

FIG. 1. (Color online) Model Description. (a) Vocal fold model. (b) Definition of the vertical stiffness gradient. (c) Schematic diagram of one glottal cycle.

about 0.12 mm with the contact pressure about 3.8 kPa, which was close to the range reported in past experiments (e.g., Verdolini *et al.*, 1999; Jiang *et al.*, 2001).

B. Glottal flow model

The glottal flow was modelled as a 1-D Bernoulli flow. The flow was assumed to separate at the minimum glottal area. Downstream of the separation point, the pressure was assumed to equal the supraglottal pressure, which was assumed to be zero gage pressure in this study. Upstream of the separation point, the pressure was solved using the Bernoulli equation:

$$p(y) = p_{\text{sub}} - \frac{1}{2}\rho_{\text{air}}\left(\frac{Q}{A(y)}\right)^2, \tag{4}$$

where $p(y)$ is the intraglottal pressure at the location y, $A(y)$ is the cross-sectional area at this location, p_{sub} is the subglottal pressure and Q is the air flow rate, and ρ_{air} is the density of air. The flow rate was calculated as

$$Q = \sqrt{\frac{2p_{\text{sub}}}{\rho_{\text{air}}}}A_{\text{min}}, \tag{5}$$

where A_{min} is the minimum area of the glottis, which is also the cross-sectional area of the glottis at the flow separation point. The coupling of the Bernoulli equation and the continuum vocal fold model was recently reported in Zhang (2015) and proved to be capable of producing reasonable results, especially when the main focus was on the vocal fold dynamics.

C. Numerical solution

The vocal fold was spatially discretized with 10-node tetrahedral elements. Grid-independence was achieved with a mesh of about 6500 non-uniform elements. For the 1-D flow, the flow domain was discretized into 100 sections in the flow direction. At each section, the transversal area was calculated by integrating the glottal width along the anterior-posterior direction.

The flow solver and solid solver were explicitly coupled. At each time step, the flow was solved with the current vocal fold position and velocity. Then the load on the vocal fold free surfaces was calculated with the obtained flow pressure. With this load, the vocal fold motion was advanced one step forward in time and the new position provided the boundary for the flow in next time step. Along with the grid-independence study, time-independence was achieved with a time-step of 5.0 e-5 s.

D. Simulation setup and data analysis

A parametric study was conducted by systematically varying the VSG and subglottal pressure. The range of the VSG based on the data in the literature was calculated and reported in Table II. In this study, the VSG was chosen to vary from 0% to 50%, which was supposed to cover the normal physiological range. The subglottal pressure was varied from 0.1 to 1.0 kPa at a 0.1 kPa increment.

TABLE II. Summary of the VSG reported in the literature (both measurements and modelling).

Source	Range
Oren *et al.* (2014a) Canine sample measurement	14.6% at 0 strain, 44% at 0.4 strain
Chhetri *et al.* (2011) Human sample measurement	estimated 43.9%
Chhetri *et al.* (2014) Canine sample measurement	23.1% ~ 71.2%
Story and Titze (1995) Three-mass model	35.30%

For each case, the simulation was carried out for a period of 0.5 s and data analysis was performed using the last 0.05 s, by which time the vocal fold motion had generally either been damped out or reached steady-state vibration. Flowrate waveforms were recorded during the simulation and the vocal fold geometry was recorded for the last one or two steady cycles. Figure 1(c) shows the schematic diagram of one glottal cycle with the time- and amplitude-based waveform measures, in which T is the period of the cycle, $t1$ is the duration of flow acceleration, $t2$ is the duration of flow deceleration, and $t3$ is the duration of glottis closure. Several essential voice quality-related quantities were computed from the waveform of the glottal flowrate, including the peak flow rate (Qmax), mean glottal flow rate (Qmean), open quotient $[(t1 + t2)/T]$, and skewness quotient $(t1/t2)$ (Holmberg *et al.*, 1988). Besides, the average flow acceleration rate was calculated as $Q\text{max}/t1$, and the average deceleration rate was calculated as $Q\text{max}/t2$. Noting that the monopole sound strength of the glottal flow is directly determined by the time-rate of the change of the flow rate ($\dot{Q}$) (Zhao *et al.*, 2002; Zhang *et al.*, 2002), the root-mean-square (RMS) value of this quantity was calculated as a measurement of the sound source strength. It needs to be pointed out that, for all the cases, cycle-to-cycle variation of these parameters over the steady-state vibration was very small, generally within 2%.

III. RESULTS AND DISCUSSION

A. Baseline cases

Simulation was first performed on the baseline model in which VSG = 0. The flow rate waveforms of the cases under different subglottal pressures are shown in Fig. 2. Several general trends were observed: (1) the peak flow rate increased with the subglottal pressure; the peak flow rate increased from 21 mL/s at 0.2 kPa subglottal pressure to 469 mL/s at 1.0 kPa subglottal pressure; (2) sustained vibration and complete glottal closure were achieved with the subglottal pressure above 0.5 kPa; at subglottal pressure of 0.4 kPa, the sustained vibration was achieved; however, the flow rate was not able to return to 0, indicating the incomplete glottal closure during the vibration; at the subglottal pressures below 0.3 kPa, the oscillation amplitude was very small, indicating that the vocal fold was just barely pushed open, and no vocal fold collision occurred; therefore, the normal phonation was considered to be achieved with the subglottal pressure above 0.5 kPa; (3) the glottal closure time increased with the

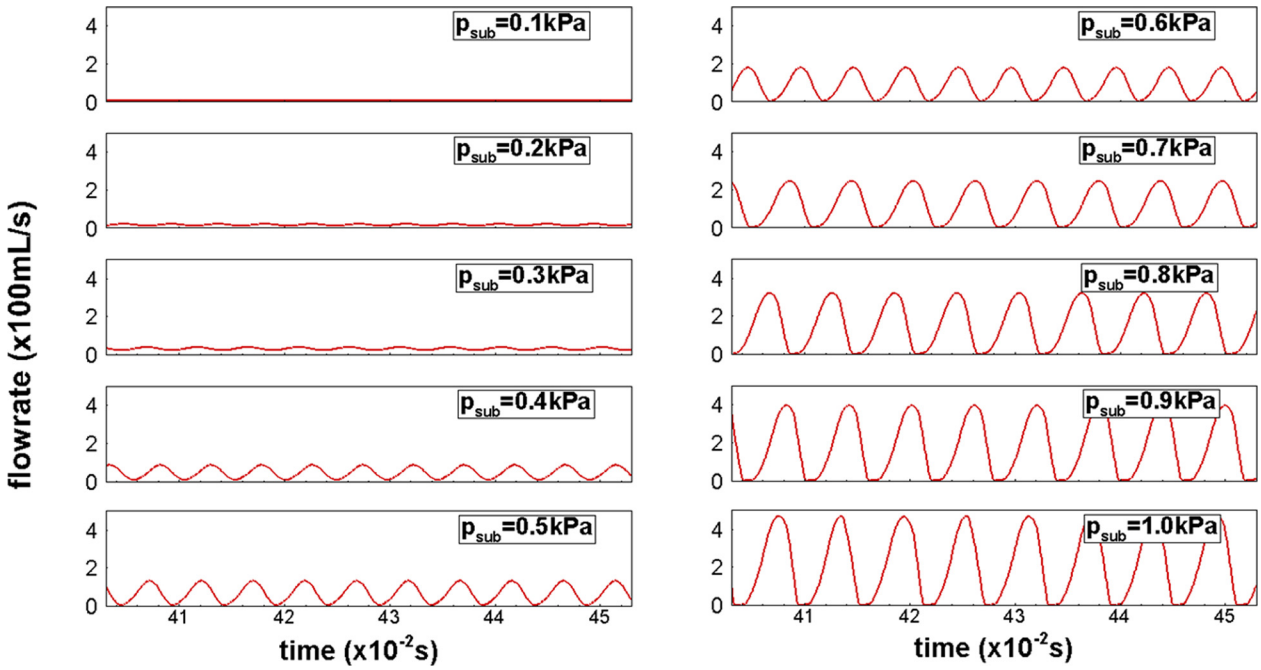

FIG. 2. (Color online) Flowrate waveforms of baseline cases.

subglottal pressure; the open quotient decreased from 0.97 to 0.84 when the subglottal pressure increased from 0.5 to 1.0 kPa. The peak flow rate, mean flow rate, skewness, and open quotients for the cases with the subglottal pressure above 0.5 kPa are shown in Table III. These parameters were found well within the physiological range (Isshiki, 1964; Hirano *et al.*, 1969; Holmberg *et al.*, 1988, 1989). It should be pointed out that at the subglottal pressure of 1.0 kPa the peak flow rate was 470 mL/s, which was slightly higher than the normal value but still acceptable given that no flow loss was considered.

Figure 3 shows the top view and mid-coronal profile of the baseline vocal fold model at 1.0 kPa subglottal pressure at six time instants during one vibration cycle. Mucosal wave propagation in the interior-superior direction was clearly seen on the medial surface of the vocal fold. The vertical phase difference was captured with the inferior aspect leading the superior aspect. The glottis presented the convergent shape during glottal opening ($t = 0.24$ T) and divergent shape during glottal closing ($t = 0.69$, 0.79 T). Furthermore, the glottis was found to open first from the anterior and posterior ends ($t = 0.24$ T) and then the middle part. Similar opening pattern was also reported in other computational and experimental studies (Zhang 2015; Mendelsohn and Zhang, 2011; Zhang, 2011; Murray and Thomson, 2012).

TABLE III. Glottal measurements of the baseline cases with normal phonation.

Psub	kPa	0.5	0.6	0.7	0.8	0.9	1.0
Qmax	mL/s	130.7	177.4	245.1	319.5	396.6	469.5
Qmean	mL/s	65.2	87.9	118.0	150.2	183.5	214.6
Skewness quotient	-	1.34	1.32	1.62	1.76	1.74	1.83
Open quotient	-	0.97	0.95	0.89	0.85	0.84	0.84

Therefore, the baseline cases showed typical glottal waveforms and vocal fold vibratory dynamics of human phonation, which served as a validation of the current model.

B. Effect of VSG on glottal flow

Figure 4 shows the peak flow rate and the relative change of the peak flow rate (ΔQmax, %) versus VSG under different subglottal pressures. It was observed that increasing VSG increased the peak flow rate, and the increase was more significant at low subglottal pressures. For example, at the 0.5 and 0.6 kPa subglottal pressures, the peak flow rate increased nearly 30% when the VSG increased from 0% to 50%, while at higher subglottal pressures the increase of the peak flow rate was below 18%. Furthermore, at 0.5 and 0.6 kPa subglottal pressures, the peak flow rate increased linearly with VSG throughout the entire range, while at higher subglottal pressures, the increase started to slow down when the VSG was beyond 30%.

Figure 5 shows the mean flow rate and the relative change of the mean flow rate (ΔQmean, %) versus VSG under different subglottal pressures. Similar to the peak flow rate, increasing VSG increased the mean flow rate, and the increase was more significant at low subglottal pressures (0.5 and 0.6 kPa). It was also interesting to notice that the relative change in the mean flow rate was much less than that in the peak flow rate. For example, at 0.5 kPa subglottal pressure, the peak flow rate increased about 29% and the mean flow rate only increased about 8% as the VSG increased from 0% to 50%. At 1.0 kPa subglottal pressure, the peak flow rate increased about 19% and the mean flow rate only increased about 5% as the VSG increased from 0% to 50%. The smaller effect on the mean glottal flow might be due to the simulation design that the overall stiffness remained the same. Nevertheless, the different effects on the

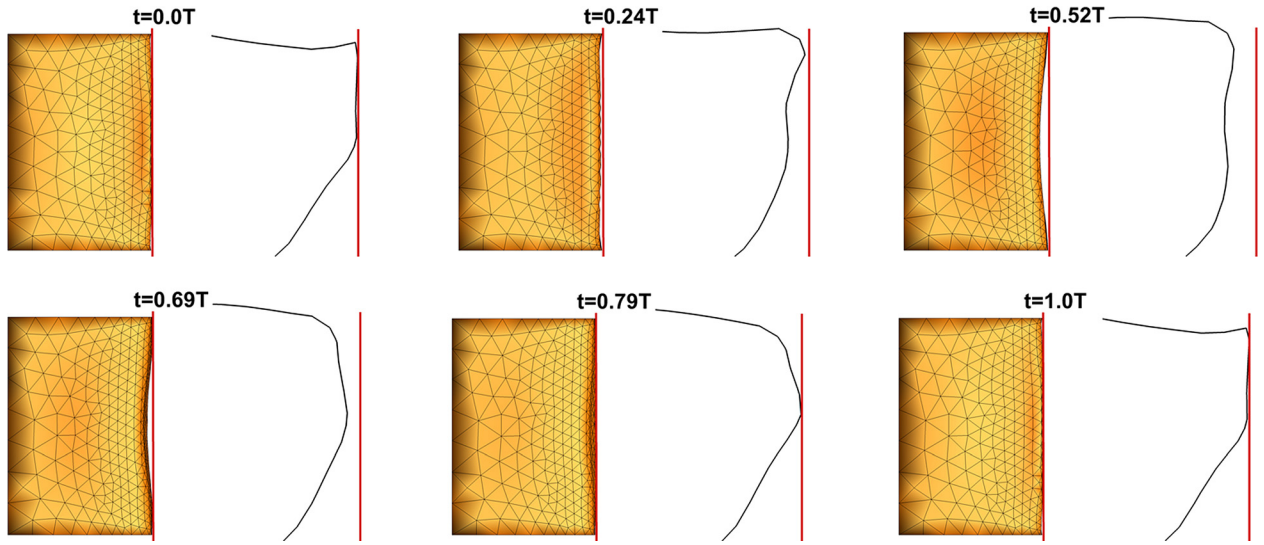

FIG. 3. (Color online) The top view and mid-coronal profile of the baseline vocal fold model at 1.0 kPa subglottal pressure at six time instants during one vibration cycle.

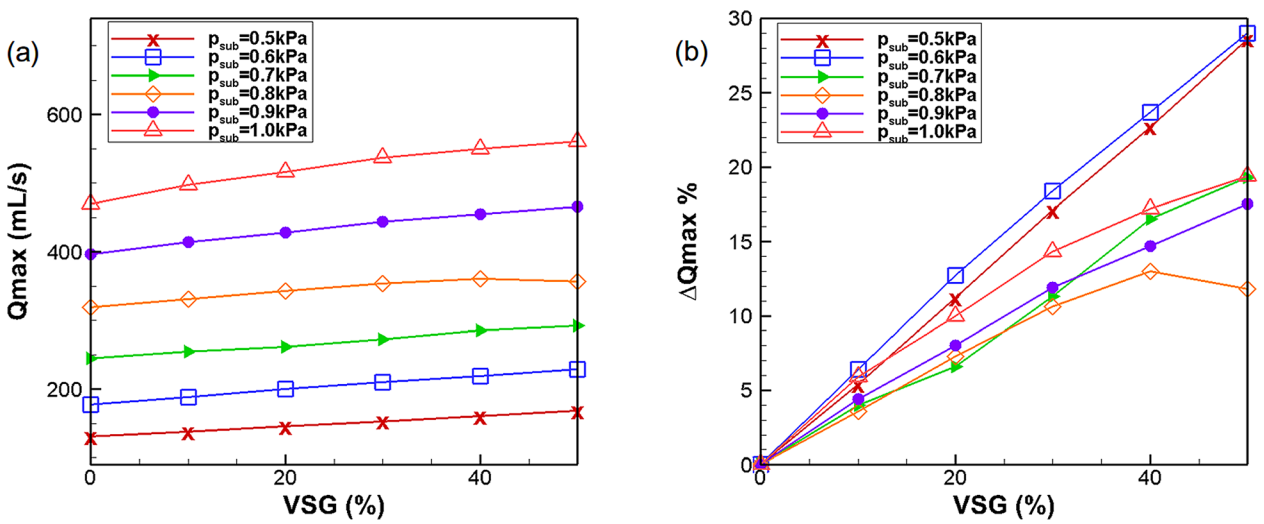

FIG. 4. (Color online) (a) The peak flow rate (mL/s) versus VSG under different subglottal pressures. (2) The relative change of the peak flow rate versus VSG under different subglottal pressures.

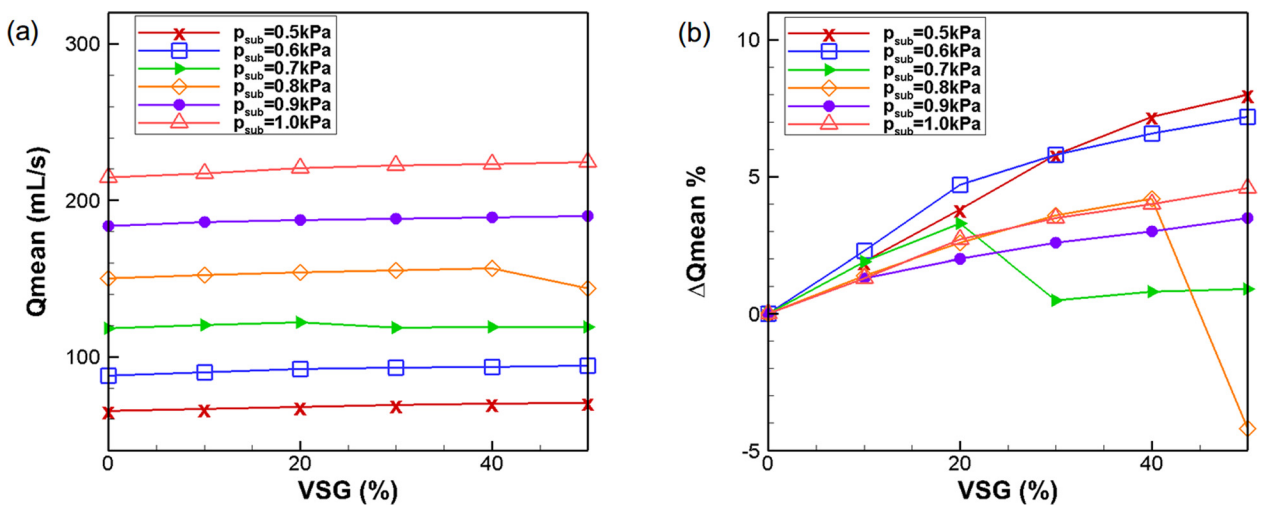

FIG. 5. (Color online) (a) The mean flow rate (mL/s) versus VSG under different subglottal pressures. (b) The relative change of the mean flow rate versus VSG under different subglottal pressures.

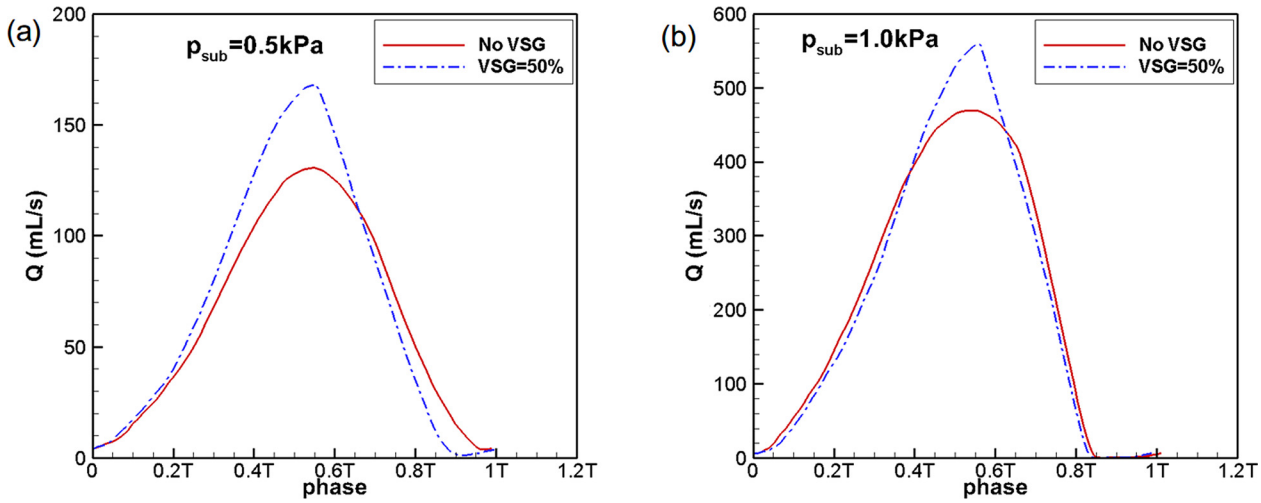

FIG. 6. (Color online) Flow rate waveforms in one cycle for the baseline case (VSG = 0) and the case with 50% VSG at 0.5 and 1.0 kPa subglottal pressures.

peak flow rate and mean flow rate suggested that the VSG had a significant effect on the waveform of the flow rate.

Figure 6 shows the flow rate waveform in one cycle for the cases at 0.5 and 1.0 kPa subglottal pressures. To better illustrate the difference, only the baseline case and the 50% VSG case are shown. The waveforms for the other VSG cases varied gradually between the two extremes. It was observed that at 0.5 kPa subglottal pressure, the flow rate in the case with VSG increased and decreased faster than that without VSG, and it reached a higher peak. At 1.0 kPa subglottal pressure, the flow rate of the two cases increased at almost the same rate before 0.4 T. After 0.4 T, while the flow rate in the case without VSG gradually slowed down, the flow rate in the case with VSG continued its high increasing rate until the peak. Therefore, the case with VSG reached a higher peak. The deceleration rate of the flow rate was almost same in the two cases. To confirm the trend under all subglottal pressures, the average flow acceleration rate and deceleration rate were calculated (Sec. II D) for all the cases and plotted in Fig. 7. Clearly, increasing VSG generally increased both acceleration and deceleration rates of the glottal flow at all subglottal pressures. Therefore, changes in the flow waveform were more concentrated toward the peak as the VSG increased. We noticed that the discrete jumps were associated with the discrete jumps of the glottal area after the vocal fold was fully opened, which generated non-smooth variation of the flow rate at the peak. This might affect the time position of the peak. However, these discrete jumps did not affect the general trend of the changing.

C. Effect of VSG on vocal fold dynamics

As the flow rate was determined solely by the glottal area in this model, the effect of VSG on the flow acceleration and deceleration suggested the effect of VSG on vocal fold vibratory dynamics. Figure 8 shows the lateral velocity contour on the mid-coronal profile of the vocal fold at three time instants in a cycle for the baseline case and the case with 50% VSG at 0.5 kPa subglottal pressure. The three time instants corresponded to the glottal opening, maximum opening and closing phases. It can be seen that the vocal fold opened from the beneath, generating a convergent glottal shape, and closed

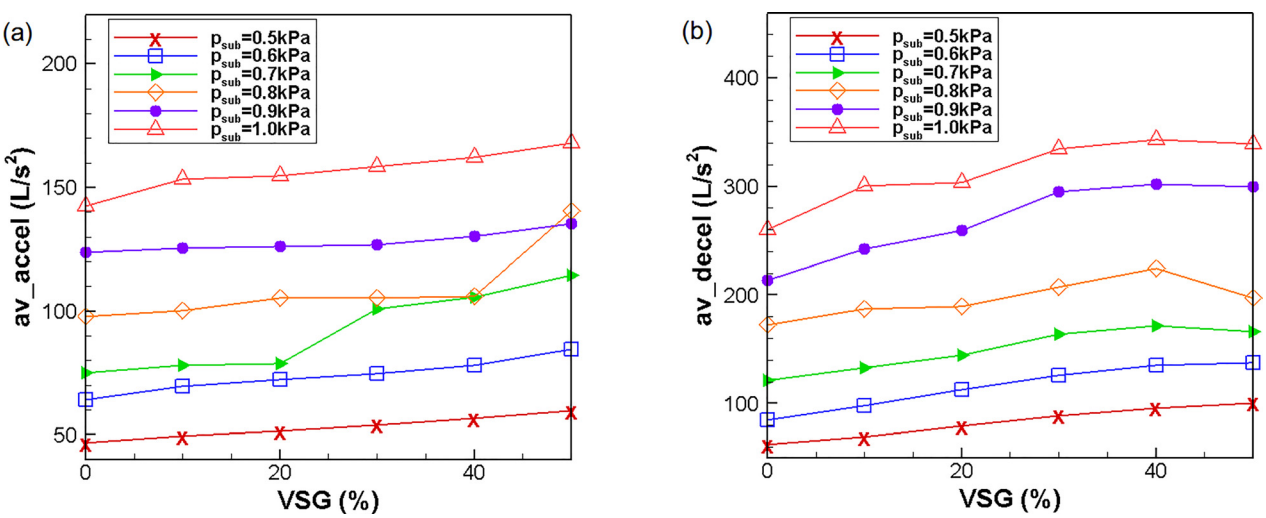

FIG. 7. (Color online) The average flow acceleration rate (L/s^2) and deceleration rate (L/s^2) versus VSG under different subglottal pressures.

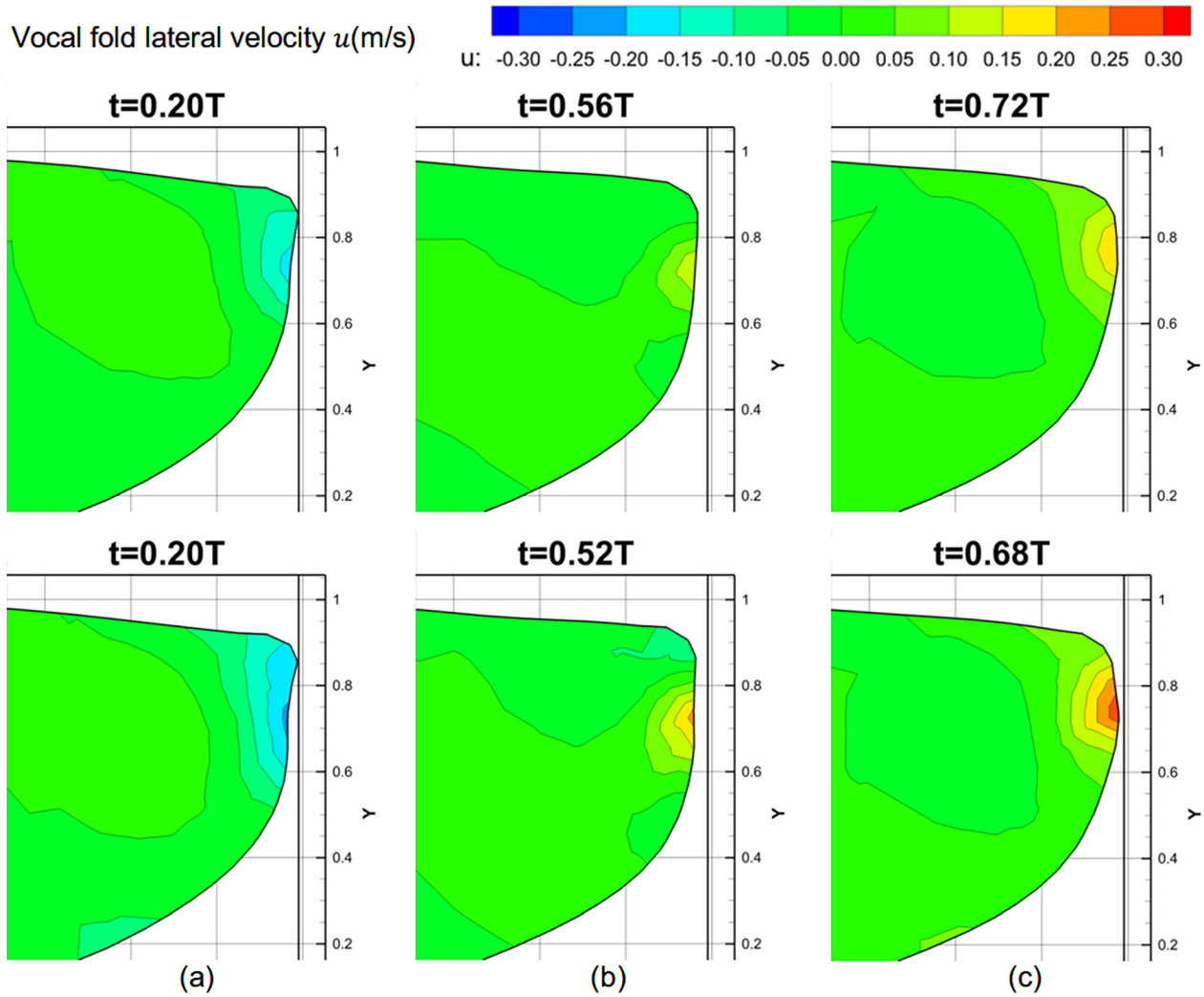

FIG. 8. (Color online) The lateral velocity contour on the mid-coronal plane of the vocal fold at three time instants in one cycle for the baseline case (top row) and the case with 50% VSG (bottom row) at 0.5 kPa subglottal pressure.

also from the beneath, generating a divergent glottal shape. It was also observed that the lateral velocity was higher in the case with VSG at all the three time instants. The highest velocity on the vocal fold surface at the three time instants was measured for the two cases. It was found that, by introducing the VSG, it increased from 0.172 to 0.216 m/s at instant (a), representing a 25.9% increase, from 0.146 to 0.217 m/s at instant (b), representing a 49.0% increase and from 0.188 to 0.288 m/s at instant (c), representing a 53.5% increase. The higher velocity indicated faster opening and closing of the vocal folds, which was consistent with the faster acceleration and deceleration of the flow, as seen in Fig. 6(a). We speculated that the increased vocal fold velocity was associated with the softened superior aspect of the vocal fold. As the superior aspect became softer, it was less resistant to the aerodynamic force, so it was easier to be pushed apart during glottis opening, especially at the beginning cycles of the vibration, resulting in larger vibrations. The larger vibration caused higher vocal fold velocities. It also resulted in higher peak flow rate. However, the speculation needs to be verified in future studies. It should be pointed out that, while the reduced stiffness at the superior aspect may generate larger vibrations, the increased stiffness at the inferior part was important for maintaining the overall stiffness of the vocal fold so that the mean flow rate was not affected, and this is important for maintaining the speech time during breath.

Figure 9 shows the lateral velocity contour on the mid-coronal profile of the vocal fold at three time instants in a cycle for the baseline case and the case with 50% VSG at 1.0 kPa subglottal pressure. Higher velocity was also observed in the case with VSG. The highest velocity on the vocal fold surface at the three time instants was measured for the two cases. By introducing the VSG, it increased from 0.521 to 0.604 m/s at instant (a), representing a 16.0% increase, from 0.332 to 0.515 m/s at instant (b), representing a 54.9% increase and from 0.616 to 0.689 m/s at instant (c), representing an 11.9% increase. It was noticed that the velocity increase was not as significant as that at 0.5 kPa subglottal pressure. The reason might be that the vocal fold vibration was the balanced effect of the aerodynamics force (subglottal pressure) and vocal fold elastic force (stiffness); as the subglottal pressure increased from 0.5 to 1.0 kPa, the influence of the stiffness change was weakened. This also explained why the flow acceleration and deceleration rate was not affected much at 1.0 kPa subglottal pressure by introducing the VSG, as seen in Fig. 6(b).

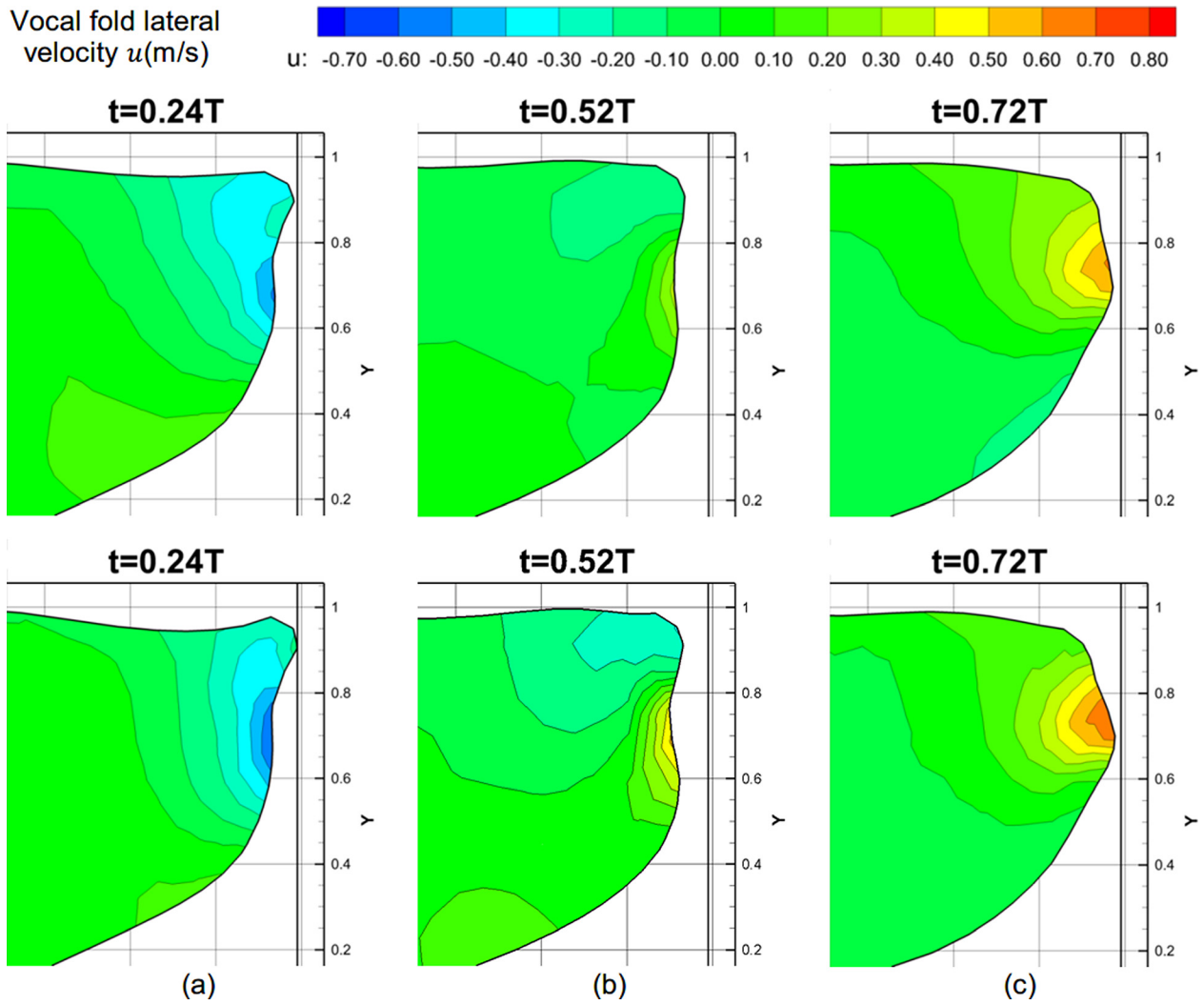

FIG. 9. (Color online) The lateral velocity contour on the mid-coronal plane of the vocal fold at three time instants in one cycle for the baseline case (top row) and the case with 50% VSG (bottom row) at 1.0 kPa subglottal pressure.

The velocity change on the medial surface of the vocal fold would also affect the vertical phase difference during the vibration. Figure 10 shows the time history of the displacement of two tracking points at the superior and inferior aspects, respectively, on the mid-coronal plane of the vocal fold for the cases at 0.5 and 1.0 kPa subglottal pressures. To better illustrate the difference, only the baseline case and the 50% VSG case are shown. The vertical phase difference was calculated as the ratio of the lag between the peak displacements of the two points to the period. It was observed that at 0.5 kPa subglottal pressure the vertical phase difference increased from 0.17 to 0.20 T by increasing the VSG from 0% to 50%, representing a 3% increase. At 1.0 kPa subglottal pressure the vertical phase difference increased from 0.19 to 0.25 T by increasing the VSG from 0% to 50%, representing a 6% increase. Therefore, increasing VSG increased the vertical phase difference. It should be pointed out that the value of the vertical phase difference depended on the position of the chosen points on the vocal fold. Different points would generate different values. However, it should not affect the general trend.

Increased vertical phase difference implied more distinct divergent angle during vocal fold vibration. To illustrate this effect, the maximum divergent angle (the angel between vocal fold medial surface and the glottal midline) during the vocal fold vibration was measured at the mid-coronal plane of the vocal fold. The maximum divergent angle versus VSG under different subglottal pressures is shown in Fig. 11. It confirmed that the divergent angle increased with the increasing VSG at all subglottal pressures. Larger divergent angels are important for the development of the intraglottal flow separation, which might facilitate phonation by lowering the threshold pressure (Zhang, 2008). The divergent angle was also observed to increase with the increasing subglottal pressure, which was consistent with past experimental observations (Oren *et al.*, 2014b). But different from the authors' hypothesis (Oren *et al.*, 2014a) that it was due to the VSG introduced under high subglottal pressures, this could happen without the presence of VSG.

D. Effect of VSG on sound production

Figure 12(a) shows the open quotient versus VSG under all subglottal pressures. The open quotient decreased with the increasing VSG under lower subglottal pressures (0.5–0.7 kPa), and remained almost constant under higher subglottal pressures

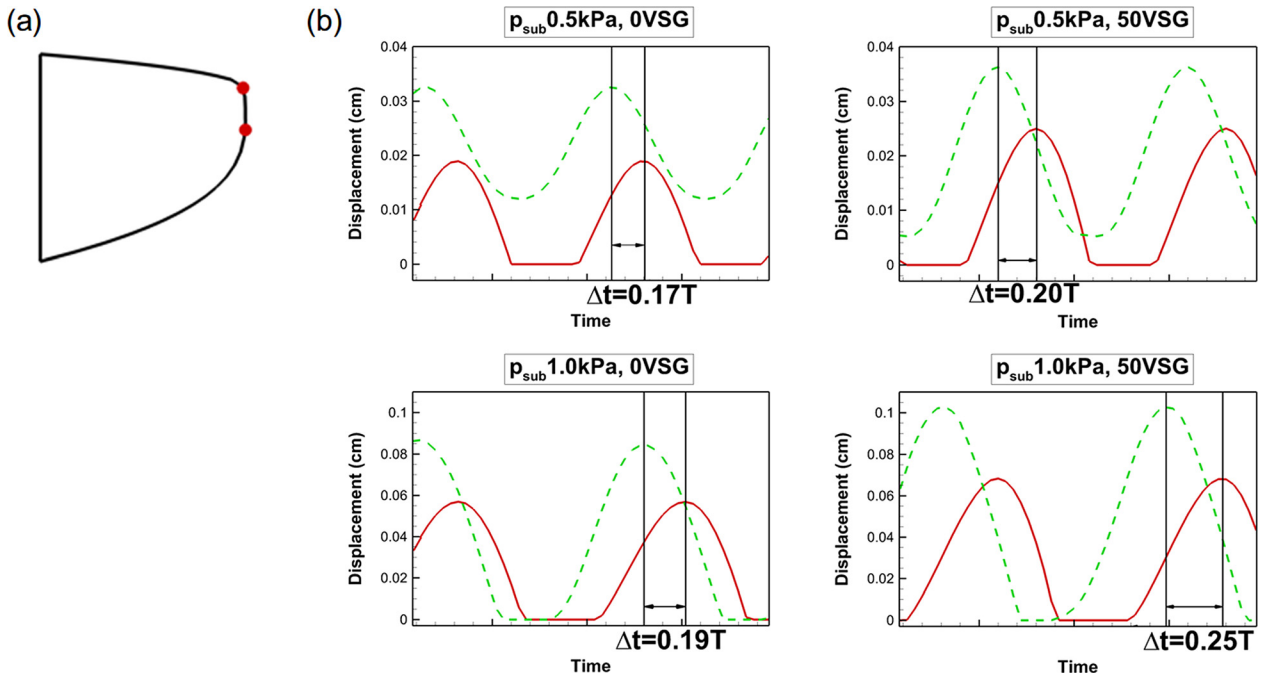

FIG. 10. (Color online) (a) The location of the two tracking points on the mid-coronal plane of the vocal fold. (b) The time history of the displacement of the superior point (solid line) and the inferior point (dashed line) for the cases at 0.5 and 1.0 kPa subglottal pressures.

(0.8–1.0 kPa). It was consistent with the observations in Figs. 6 and 8. Under low subglottal pressures, increasing VSG largely increased the vocal fold vibration, resulting in faster opening and closing, and thereby shortened the overall duration of glottal opening ($t1 + t2$), as seen in Fig. 6(a). However, under high subglottal pressures (large aerodynamic force), the influence of the stiffness change was weakened, and thus the overall duration of the glottal opening was not affected much, as seen in Fig. 6(b).

Figure 12(b) shows the RMS value of the time rate of the change of the glottal flow rate ($\dot{Q}$) versus VSG under all subglottal pressures. $\dot{Q}$ is directly related to the sound strength of the glottal jet. It is seen that that $\dot{Q}$ generally increased with the increasing VSG, which indicated that increasing VSG would generate a stronger sound source. It was also noticed in Fig. 6 that as the VSG increased from 0 to 50, the flow rate waveform became pointy at the peak. Similar waveform changes were reported from the measurements in human subjects by Holmberg *et al.* (1988). They showed that with the increased loudness, the flow rate waveform changed from the more flattened and rounded shape to the more uplifted and peaky shape. Therefore, the waveform change with increased VSG also indicated that increasing VSG would increase sound intensity. Besides the increase in the sound source strength, increasing VSG can also possibly reduce the threshold pressure. For example, at the subglottal pressure of 0.3 kPa, when the VSG increased from 0 to 50, the value of $\dot{Q}$ increased from nearly 0 L/s^2 to 30 L/s^2.

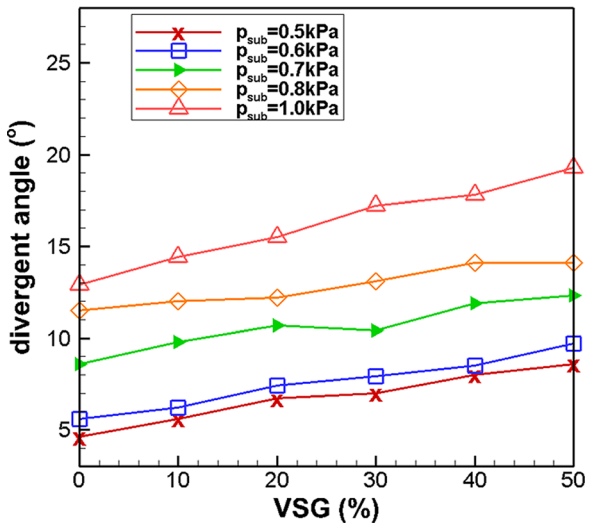

FIG. 11. (Color online) The maximum divergent angle versus VSG under different subglottal pressures.

IV. CONCLUSION

A. Summary and implication

Parametric flow-structure interaction simulations with coupled a continuum vocal fold model and a 1-D Bernoulli flow model have been carried out to study the effect of the vertical stiffness variation on vocal fold dynamics and sound production. Key observations included:

(1) Increasing VSG would increase the peak flow rate and sound intensity and decrease the open quotient and threshold pressure. The effect was found to be more prominent at low subglottal pressures.
(2) Increasing VSG resulted in larger vibrations and higher vocal fold velocities. We speculated that it was due to the reduced stiffness at the superior aspect of the vocal fold which made the glottis opening easier and resulted in larger vibrations.

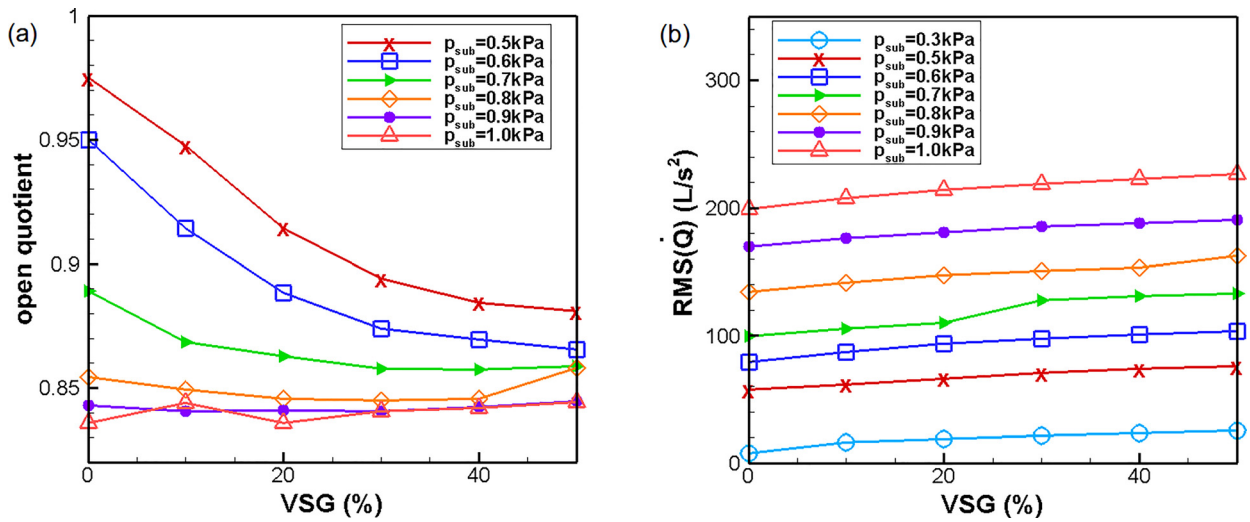

FIG. 12. (Color online) (a) The open quotient versus VSG under different subglottal pressures. (b) The RMS of $\dot{Q}$ (L/s^2) versus VSG under different subglottal pressures.

(3) Increasing VSG only increased the mean flow rate slightly, which is important to maintain the speech duration during breath.
(4) Increasing VSG increased the vertical phase difference and divergent angel during the vocal fold vibration, which would benefit the development of intraglottal flow separation.

The results have implication for clinical practice. It might be more important to maintain the soft superior part in vocal fold medialization surgeries, which can be achieved through specific-shaped implants (Orestes *et al.*, 2014) and/or inserting the implant to a lower location. However, the inferior aspect should not be made excessive stiff, otherwise the fold will be too stiff to be pushed apart.

B. Limitations and future work

At last, it is useful to point out the limitations of the current work. First, the current flow model did not include the flow viscous effects. Although the viscous force was generally one-order of magnitude smaller than the pressure force, it may be still large enough to affect the vocal fold dynamics. Furthermore, in the current study, the glottal flow was assumed to be separated at the minimum glottal area, while the actual flow separation point could be different in the real condition. This certainly affected the distribution of the aerodynamic loading. Second, all the three moduli were varied together, which might not be realistic. Third, due to the method used to quantify the vertical stiffness variation, the inferior part and superior part were varied simultaneously, making it difficult to distinguish their separate effects. Besides, the VSG was only increased to 50%. The general trends reported so far may not hold when the VSG is further increased. Future work would couple the current model with the acoustic model to quantify the effect of VSG on acoustic measurements. Besides, direct modelling of the conus elasticus and its fixation to the cartilaginous walls would help to identify the cause of the vertical stiffness variation.

ACKNOWLEDGMENT

The research described was supported by Grant No. 1R03DC014562 from the National Institute on Deafness and Other Communication Disorders (NIDCD). The authors also thank Dr. Sid Khosla for the discussion regarding the stiffness variation.

Alipour, F., Berry, D. A., and Titze, I. R. (**2000**). "A finite-element model of vocal fold vibration," J. Acoust. Soc. Am. **108**(6), 3003–3012.
Chhetri, D. K., and Rafizadeh, S. (**2014**). "Young's modulus of canine vocal fold cover layers," J. Voice **28**(4), 406–410.
Chhetri, D. K., Zhang, Z., and Neubauer, J. (**2011**). "Measurement of Young's modulus of vocal folds by indentation," J. Voice **25**(1), 1–7.
Dembinski, D., Oren, L., Gutmark, E., and Khosla, S. (**2013**). "Elasticity measurements in the superior/inferior aspects of the vocal folds," in *10th International Conference Advances in Quantitative Laryngology*, p. 65.
Hirano, M., Ohala, J., and Vennard, W. (**1969**). "The function of laryngeal muscles in regulating fundamental frequency and intensity of phonation," J. Speech, Lang., Hear. Res. **12**(3), 616–628.
Holmberg, E. B., Hillman, R. E., and Perkell, J. S. (**1988**). "Glottal airflow and transglottal air pressure measurements for male and female speakers in soft, normal, and loud voice," J. Acoust. Soc. Am. **84**(2), 511–529.
Holmberg, E. B., Hillman, R. E., and Perkell, J. S. (**1989**). "Glottal airflow and transglottal air pressure measurements for male and female speakers in low, normal, and high pitch," J. Voice **3**(4), 294–305.
Isshiki, N. (**1964**). "Regulatory mechanism of voice intensity variation," J. Speech, Lang., Hear. Res. **7**(1), 17–29.
Jiang, J. J., Shah, A. G., Hess, M. M., Verdolini, K., Banzali, F. M., and Hanson, D. G. (**2001**). "Vocal fold impact stress analysis," J. Voice **15**(1), 4–14.
Mendelsohn, A. H., and Zhang, Z. (**2011**). "Phonation threshold pressure and onset frequency in a two-layer physical model of the vocal folds," J. Acoust. Soc. Am. **130**(5), 2961–2968.
Murray, P. R., and Thomson, S. L. (**2012**). "Vibratory responses of synthetic, self-oscillating vocal fold models," J. Acoust. Soc. Am. **132**(5), 3428–3438.
Oren, L., Dembinski, D., Gutmark, E., and Khosla, S. (**2014a**). "Characterization of the vocal fold vertical stiffness in a canine model," J. Voice **28**(3), 297–304.
Oren, L., Khosla, S., and Gutmark, E. (**2014b**). "Intraglottal geometry and velocity measurements in canine larynges," J. Acoust. Soc. Am. **135**(1), 380–388.
Orestes, M. I., Neubauer, J., Sofer, E., Salinas, J., and Chhetri, D. K. (**2014**). "Phonatory effects of type I thyroplasty implant shape and depth of medialization in unilateral vocal fold paralysis," Laryngoscope **124**(12), 2791–2796.

Reidenbach, M. M. (**1996**). "The attachments of the conus elasticus to the laryngeal skeleton: Physiologic and clinical implications," Clin. Anat. **9**(6), 363–370.
Story, B. H., and Titze, I. R. (**1995**). "Voice simulation with a body-cover model of the vocal folds," J. Acoust. Soc. Am. **97**(2), 1249–1260.
Verdolini, K., Hess, M. M., Titze, I. R., Bierhals, W., and Gross, M. (**1999**). "Investigation of vocal fold impact stress in human subjects," J. Voice **13**(2), 184–202.
Zhang, C., Zhao, W., Frankel, S. H., and Mongeau, L. (**2002**). "Computational aeroacoustics of phonation, Part II: Effects of flow parameters and ventricular folds," J. Acoust. Soc. Am. **112**(5), 2147–2154.
Zhang, Z. (**2008**). "Influence of flow separation location on phonation onseta)," J. Acoust. Soc. Am. **124**(3), 1689–1694.
Zhang, Z. (**2011**). "Restraining mechanisms in regulating glottal closure during phonation," J. Acoust. Soc. Am. **130**(6), 4010–4019.
Zhang, Z. (**2015**). "Regulation of glottal closure and airflow in a three-dimensional phonation model: Implications for vocal intensity control," J. Acoust. Soc. Am. **137**(2), 898–910.
Zhao, W., Zhang, C., Frankel, S. H., and Mongeau, L. (**2002**). "Computational aeroacoustics of phonation, Part I: Computational methods and sound generation mechanisms," J. Acoust. Soc. Am. **112**(5), 2134–2146.
Zheng, X., Xue, Q., Mittal, R., and Beilamowicz, S. (**2010**). "A coupled sharp-interface immersed boundary-finite-element method for flow-structure interaction with application to human phonation," J. Biomech. Eng. **132**(11), 111003.